Article

RXFP2-positive mesenchymal stem cells in the antlerogenic periosteum contribute to postnatal development of deer antlers

Check for updates

Hengxing Ba [1,5] ✉, Pengfei Hu [1,5], Hongming Yuan [2,5], Chao Ma[1], Zhen Wang[1], Yudong Shang[1], Qianqian Guo [1], Datao Wang [3] & Chunyi Li [1,4] ✉

The postnatal development of secondary sexual characteristics is a highly complex process governed by diverse molecular signals and serves as a key marker of sexual maturity. Deer antlers exemplify such traits, distinguished not only by their unique ability to regenerate annually but also by their initiation in postnatal life. It is well established that the antlerogenic periosteum (AP) is the only tissue responsible for postnatal antler formation. Here, we identify a population of RXFP2-positive mesenchymal stem cells within the AP of both male and female deer that are crucial for antler development, primarily through the activation of canonical Wnt signaling. This process also relies on M2 macrophages recruited via IL-34 secretion. Furthermore, these cells exhibit reduced expression of HOX genes, suggesting a high degree of developmental plasticity. Our findings offer new insights into the molecular mechanisms underlying the postnatal development of secondary sexual characteristics, using deer antlers serving as a model system.

The postnatal development of secondary sexual characteristics is an exceedingly complex and diverse molecular signaling process and serves as a hallmark of sexual maturity[1]. Interestingly, most of the secondary sexual characteristics during puberty build up from their miniature prototypes under the stimulation of sex hormones. For instance, dark and thick beards, a male secondary sexual characteristic, are transformed from tiny, pale, vellus hairs, under the stimulation of androgen hormones[2–4]. Morphologically and functionally distinct breasts, a female secondary sexual characteristic, are developed from the rudimentary mammary glands (even with some secretion activities) under the stimulation of estrogen hormones[5]. In contrast, the deer antler, a typical male secondary sexual characteristic, is developed from a small (around 1–2 mm in thickness and 2.5–3 cm in diameter) and simple (consisting of cambium and fibrous layers) piece of periosteum, namely antlerogenic periosteum (AP)[6,7] during puberty. Even more so, once generated, antlers have gained the ability of annual full regeneration, the only case among mammalian appendages. We believe that understanding the molecular mechanisms behind how such a large, complicated, and species-specific secondary sexual characteristic can develop from a small and simple tissue under androgen stimulation presents a unique opportunity. This knowledge could help address fundamental

questions regarding the development of secondary sexual characteristics and the occurrence of abnormalities during puberty, using the extreme model of deer antlers.

The deer antler has been described as an "improbable" appendage by developmental biologists because it possesses some unique biological attributes that contrast with typical mammalian appendages and it may hold the key to some fundamental biological questions[8–11]. Among these attributes, the antler features annual full regeneration[8–12] and an unprecedented growth rate[13–15], both of which have been intensively studied, whereas some other aspects have been relatively neglected. For example, as an embryonic appendage, pedicle development is initiated around 100 days of gestation, evidenced by the skin thickening in the presumptive region, due to transient activation of the testicular axis, but this development is short-lived and the pedicle is not usually apparent at birth[6,16]. True antler growth commences only when a male deer approaches puberty and is triggered by significantly elevated androgen hormones[17,18] that stimulate pedicle development from which the first antler then grows. Therefore, antlers are male secondary sexual characteristics and their development is under the control of androgens.

Through a combination of tissue deletion and transplantation experiments, the AP that overlies the presumptive pedicle growth region

[1]Jilin Provincial Key Laboratory of Deer Antler Biology, Institute of Antler Science and Product Technology, Changchun Sci-Tech University, Changchun, 130600, China. [2]Jilin Provincial Key Laboratory of Institute of Zoonoses, Animal Genome Editing Technology Innovation Center, College of Animal Sciences, Jilin University, Changchun, 130062, China. [3]Institute of Special Animal and Plant Science, Chinese Academy of Agricultural Sciences, Changchun, 130112, China. [4]College of Chinese Medicinal Materials, Jilin Agricultural University, Changchun, 130118, China. [5]These authors contributed equally: Hengxing Ba, Pengfei Hu, Hongming Yuan. ✉e-mail: bahengxing@cstu.edu.cn; lichunyi1959@163.com

(centered in the frontal crest) has been identified as the key tissue type for the initiation of the pedicle and then formation of the first antler[8]. Pedicles are permanent bony protuberances, from which antlers are cast and regenerate[19]. Deletion of the AP abolishes future pedicle development, whereas transplantation of the AP induces ectopic pedicle and antler formation[6,7,20,21]. Further investigations revealed that AP can initiate the development of xenogeneic pedicles[22] and even xenogeneic antlers[23] when AP tissues are transplanted onto nude mice, an immune-deficient animal model. Therefore, the AP is a unique type of tissue that possesses autonomous self-differentiation ability. Interestingly, under exogenous androgen stimulation, female deer can also grow pedicles and subsequent antlers[17], indicating that female deer also possess the capable AP.

We have characterized the AP cells histologically[19] and ultrastructurally[24], and found that they resemble embryonic cells in some aspects, such as the rich distribution of glycogen within their cytoplasm. An in vivo study further confirmed their embryonic nature as cultured donor cell lines derived from male AP (whether left undifferentiated or chemically induced to initiate osteogenesis or adipogenesis) was used in the successful cloning, in which AP cells partially incorporated into some organ development[25]. Because of the AP cells in vitro can self-renew, differentiate into multiple cell lineages, and express typical mesenchymal stem cell as well as key embryonic stem cell markers[26–28], we have termed them antler mesenchymal stem cells[27].

Recently, we carried out single-cell RNA sequencing (scRNA-seq) of the AP tissue and found that AP cells are heterologous with at least eight cell populations[29]. Among them, the THY1$^+$ mesenchymal stem cells (THY1$^+$ APMCs) highly expressed pluripotent stem cell markers and differentiated into AP progenitor cells (APPCs). We found that THY1$^+$ APMCs highly expressed androgen hormone receptor (AR) plus its downstream target gene, the relaxin family peptide receptor 2 (RXFP2)[30]. The latter is found to be the sole factor involved in the phenotype of sheep horns[31] and there is evidence to believe that RXFP2 may also be an indispensable factor that is involved in the phenotype of deer antlers, another type of ungulate headpiece[29,32]. Based on these findings, we hypothesize that THY1$^+$RXFP2$^+$ APMCs represent the core cell type responsible for initiating the postnatal development of antlers and that RXFP2$^+$ APMCs are regulated by the AR-RXFP2 signaling axis. However, our in vitro investigations[33] revealed that androgen hormones do not exert direct mitogenic effects on the AP cells, which raise the possibility that other players are involved to mediate androgen action. We believe these intermediate players cannot be identified unless pure populations of RXFP2$^+$ APMCs are isolated and subject to gain- or loss-of-function investigations.

In this study, we took multiple approaches: (1) to analyze scRNA-seq as well as bulk RNA-seq data for male and female deer AP, deer facial periosteum (FP), and deer long bone periosteum (LP) tissues (Fig. 1A) to determine whether THY1$^+$RXFP2$^+$ APMCs in the male and female AP are a uniquely AP reserved cell subpopulation that differ from THY1$^+$ cells in the FP and LP tissues; (2) to isolate a pure population of RXFP2$^+$ APMCs and to identify the potential activation signaling pathways via loss-of-function assay; (3) to fully characterize RXFP2$^+$ APMCs (cranial neural crest cell (CNCC)-derived) and to compare them with bone marrow-derived mesenchymal stem cells (BMSCs; mesoderm-derived) in seeking to reveal their unique attributes. This study sought to uncover novel insights at the cellular and molecular levels into the regulation of RXFP2$^+$ APMCs, potentially shedding light on the mechanism underlying the situation of postnatal development of secondary sexual characteristics, using deer antlers as a model system.

Results
RXFP2$^+$ cells identified only in the AP of both male and female
To identify the exclusive cell population in the AP of male and female deer via highly expressed genes, we compared bulk RNA-seq data of male and female AP with those of FP tissue, respectively. The results showed that expression of the RXFP2 gene was up-regulated significantly in both male and female AP (Fig. 1B and Supplementary Fig. 1), although in female AP

expression was lower than in male AP, with a $\log_2$FoldChange of –2.3 and an adjusted p of 0.006. This differential expression was further validated at the protein level ($p < 0.05$, Fig. 1C). Furthermore, in comparison with our previously published bulk RNA-seq data from various tissue types, we found that high level expressions of RXFP2 were exclusive to male and female AP tissues (Fig. 1D). In the pedicle periosteum (PP, the tissue for antler regeneration) and antler tip reserve mesenchyme (the tissue for rapid antler elongation), both of which are AP-derived tissues, RXFP2 expression was significantly down-regulated; it was not detectable in the other 17 deer tissue types analyzed (Fig. 1D). Cross-species analysis revealed that high level expression of RXFP2 was specifically detected in the AP of antlered deer species including sika deer, wapiti, and reindeer, but not in the equivalent AP of Chinese water deer, antler-less deer species (Fig. 1E). These results indicate that RXFP2 is specifically expressed in the AP tissue of antlered deer.

To determine whether RXFP2 expression is specific to a particular cell subpopulation in the AP cells, we conducted an unsupervised clustering analysis on the scRNA-seq data from four types of periosteum: male and female AP, FP and LP. In the analysis, we identified nine clusters for male AP, eight clusters for female AP, eight clusters for FP, and seven clusters for LP tissues (Fig. 2A). Using established gene markers[29], we defined cell types from these clusters, including THY1$^+$ mesenchymal stem cells in AP (APMCs), FP (FPMCs) and LP (LPMCs), respectively; and RUNX2$^+$ APPCs, ACTA2$^+$ vascular smooth muscle cells and pericytes, CDH5$^+$ vascular endothelial cells, MMRN1$^+$ lymphatic endothelial cells, KIT$^+$ mast cells, CSF1R$^+$ macrophages, CD3E$^+$ T cells, and ALPL$^+$ osteochondroblasts. Not unexpectedly, we found that RUNX2$^+$ APPCs in male AP accounted for a large proportion of proliferative cells (Fig. 2A, Supplementary Fig. 2, Supplementary Fig. 3).

For all four types of periosteal tissue, THY1$^+$ cells could be divided into two subclusters through unsupervised clustering: THY1$^+$ C0 and THY1$^+$ C1 (Fig. 2A). Interestingly, RXFP2 expression was exclusively detected in THY1$^+$ C1 from both male and female AP tissues (Fig. 2B), leading to a delineation of distinct subpopulations within THY1$^+$ APMCs. However, PRRX1, previously identified as a marker gene for the mesenchymal cell population driving antler regeneration[34] and TWIST1, a widely used mesenchymal signature gene[35], were both expressed in all THY1$^+$ mesenchymal cells across the four tissue types (Fig. 2B). Therefore, RXFP2$^+$ cells are more specific to antlerogenesis than previously identified marker genes, such as PRRX1. Additionally, RNA velocity analysis of male AP scRNA-seq data further revealed the differentiation trajectory from THY1$^+$ C1 to APPCs (Fig. 2C). Therefore, we concluded that THY1$^+$RXFP2$^+$ APMCs, which is found exclusively in the AP of both male and female deer, must be the key cell type responsible for postnatal development of antlers.

Activation of RXFP2$^+$ APMCs requires involvement of canonical Wnt signaling
To explore the molecular mechanism underlying the activation of RXFP2$^+$ APMCs for postnatal development of antlers, we carried out a comparative global transcriptome profiling of four types of periosteal tissue and revealed that the acquired clusters could be classified into two distinct groups (Fig. 3A). Group 1 consisted of male and female AP THY1$^+$ C0, FP THY1$^+$ C0, and LP THY1$^+$ C0 and LP THY1$^+$ C1. Group 2 comprised male and female AP THY1$^+$ C1 and FP THY1$^+$ C1. Next, we identified a total of 119 non-redundant highly expressed genes shared between THY1$^+$ clusters in Group 2 (Fig. 3B). These genes are found to be implicated in cell division (e.g., TGFB2, PDGFD, IGF2, PTN, THBS4), response to xenobiotic stimuli (e.g., FZD1, NPPC, TGFB2, SFRP2, FOSB, NFATC2, INHBA, THBS1), ossification (e.g., NPPC, COL11A1, CLEC11A, IGF2, RUNX2) as well as negative regulation of canonical Wnt signaling (e.g., SFRP2, SFRP4, DKK2, and DKK3) (Fig. 3C). We found that Wnt signaling inhibitors exhibited significantly higher expression levels in male and female THY1$^+$ C1 compared to their correspondent THY1$^+$ C0, and the expression levels of these inhibitors were reduced in APPCs (Fig. 3D). This indicates that Wnt signaling was activated during differentiation from AP THY1$^+$ C1 to APPCs.
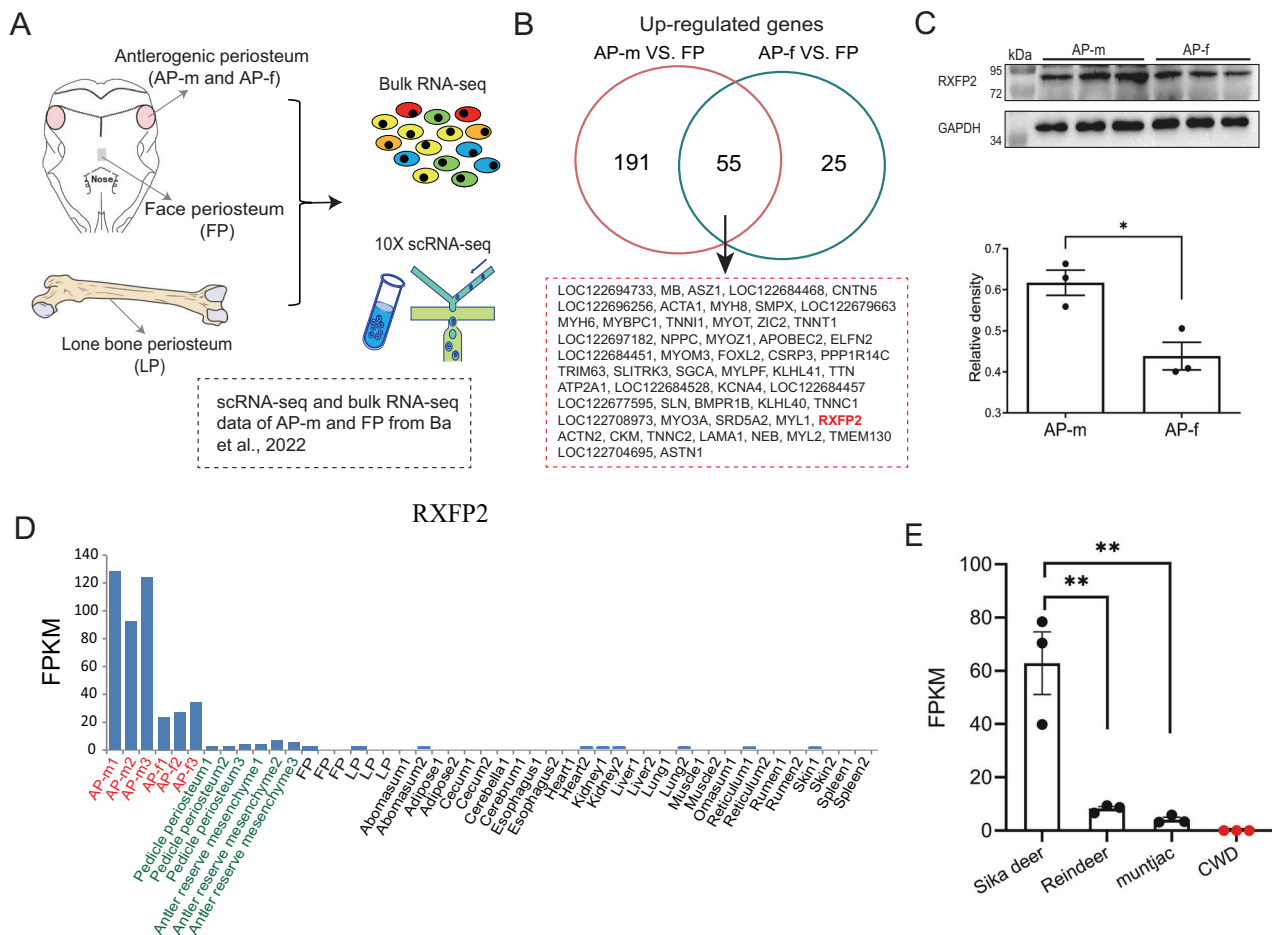
Fig. 1 | RXFP2 only expressed in male and female antlerogenic periosteum.
A Schematic showing the locations of antlerogenic periosteum (AP), facial periosteum (FP), and long bone periosteum (LP) tissues. AP-m: male AP; AP-f: female AP. **B** Venn diagram depicting upregulated genes between AP-m vs. FP and AP-f vs. FP based on $\log_2$Foldchange > 4 and adjusted $p < 0.001$. The 55 shared up-regulated genes are highlighted by a red dashed box, with RXFP2 specifically highlighted in red. **C** Immunoblots of RXFP2 protein in AP-m and AP-f tissues, with GAPDH as the internal reference protein. Relative intensity of each immunoblot was calculated using Image J. *$p < 0.05$. Error bars indicate the SEM. **D** Expression levels (FPKM) of RXFP2 across different deer tissues. Both AP-m and AP-f tissues are highlighted in red, and AP-derived tissues (pedicle periosteum and antler reserve mesenchyme) are highlighted in green. FPKM: Fragments per kilobase of transcript per million mapped fragments. **E** Expression levels (FPKM) of RXFP2 across three antlered deer species (sika deer, wapiti, and reindeer) compared to one antler-less deer species (CWD: Chinese water deer), with no detectable expression of RXFP2 observed in CWD. **$p < 0.01$. Error bars indicate the SEM.

These inhibitors only showed relatively lower expression level in LP THY1$^+$ C0 and LP THY1$^+$ C1, and there was no significant difference between these two clusters. Therefore, Wnt signaling inhibitors may play a critical role in prohibiting activation of AP THY1$^+$ C1 cells at this stage for postnatal development of antlers. The signature genes of APPCs, including TNN, TNC, PTN, and RUNX2[29,34], displayed high expression levels in AP THY1$^+$ C1 (Fig. 3E), indicating that these cells were undergoing differentiation.

We subsequently screened expression profiles for Wnt signaling receptors/co-receptors of these THY1$^+$ clusters, and found the Wnt co-receptor, LDL-receptor-related protein 6 (LRP6), were expressed at significantly higher levels in the male THY1$^+$ C1 (Fig. 4A). To confirm the involvement of Wnt signaling receptors/co-receptors in the activation of male THY1$^+$ C1, we isolated male THY1$^+$ C0 and THY1$^+$ C1 from male AP cells using flow cytometry. THY1$^+$ APMCs were isolated by staining with anti-THY1 antibody. Subsequently, the THY1$^+$ APMCs were further stained with anti-RXFP2 antibody, and THY1$^+$ C1 cells were gated for sorting. THY1$^+$ APMCs represented 86% of the total, and within this subset, 16% were double-positive for THY1 and RXFP2. We refer to male AP THY1$^+$ C0 as RXFP2$^-$ APMCs and AP THY1$^+$ C1 as RXFP2$^+$ APMCs in the following description. The isolation results were further confirmed using fluorescent immunostaining with anti-NEGR1 antibody, and NEGR1 was found to be exclusively expressed in male RXFP2$^+$ APMCs; hence, there is considerable overlap in expression between RXFP2 and NEGR1 (Fig. 4B–E, Supplementary Fig. 4A, B). CRISPR-cas9 approach was then performed to knock out the LRP6 gene (LRP6^{KO}) in male RXFP2$^+$ APMCs (Fig. 4F). Western blot analysis confirmed the loss of LRP6 expression in the knockout cell line (Fig. 4G).

Subsequent assays demonstrated the significant effects of LRP6 knockout on the activation of male RXFP2$^+$ APMCs. The cell proliferation of male RXFP2$^+$LRP6^{KO} APMCs was significantly less than that of RXFP2$^+$ APMCs, and interestingly was similar to that of RXFP2$^-$ APMCs (Fig. 4H). A greater percentage of apoptotic cells was detected in the RXFP2$^+$LRP6^{KO} APMCs (Fig. 4I), compared to the RXFP2$^+$ APMCs and RXFP2$^-$ APMCs. When cultured in the osteogenic induction medium for 21 days, male RXFP2$^+$LRP6^{KO} APMCs exhibited much weaker Alizarin Red S staining compared to that of male RXFP2$^+$ APMCs (Fig. 4J), indicating a decrease in osteogenic potential after losing LRP6, a Wnt signaling co-receptor. RXFP2$^-$ APMCs also showed low osteogenic capacity.

To further characterize the transcriptional status of male RXFP2$^+$LRP6^{KO} APMCs, we conducted bulk RNA-seq analyses on the three types of male APMCs: RXFP2$^+$, RXFP2$^-$, and RXFP2$^+$LRP6^{KO}. The results revealed a similar gene expression pattern between RXFP2$^+$LRP6^{KO} APMCs and RXFP2$^-$ APMCs (Fig. 4K). Through comparison between RXFP2$^+$ APMCs and RXFP2$^+$LRP6^{KO} APMCs (Fig. 4L), we identified 188 up-
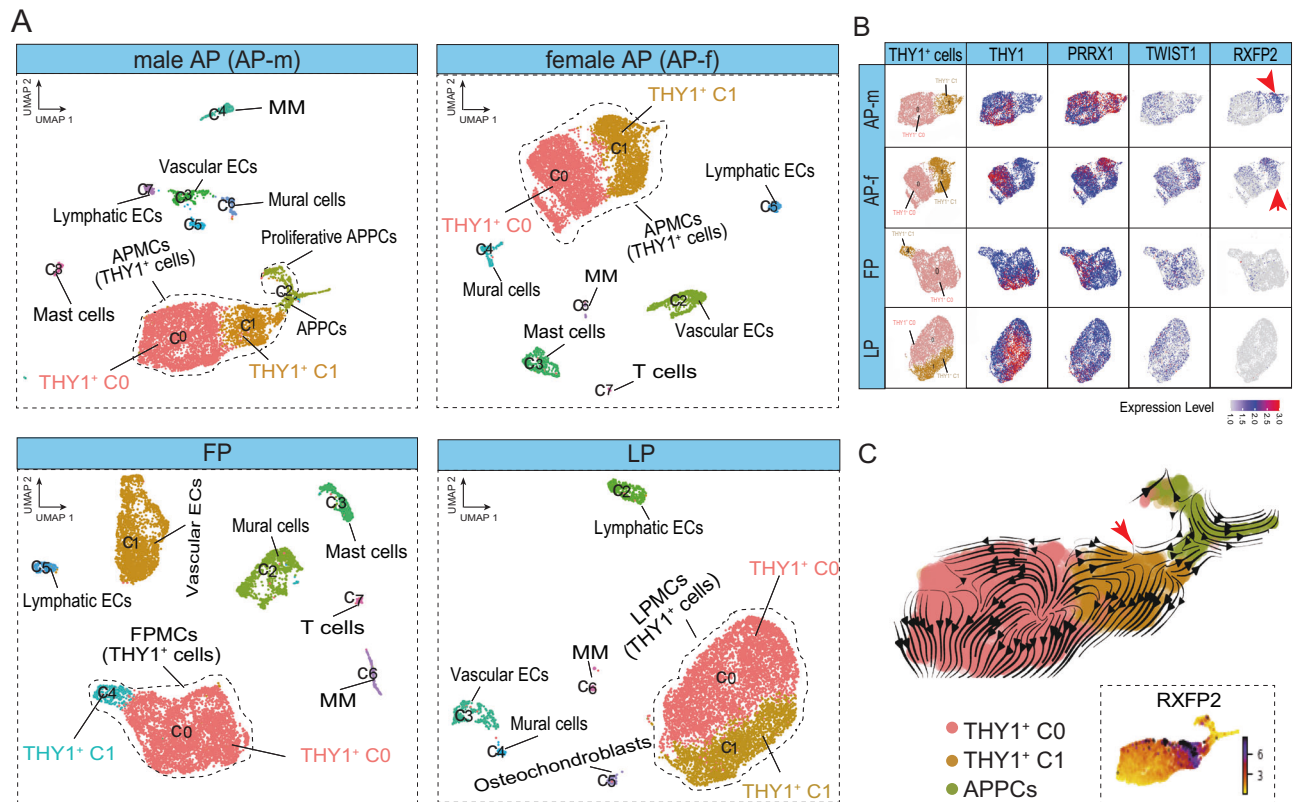
Fig. 2 | THY1+RXFP2+ cells only exist in the AP of both male and female.
A UMAP plot visualizing unsupervised clusters in each tissue: AP-m, AP-f, FP, and LP. Cell types are color-coded. Note that THY1+ mesenchymal cells in each tissue are assigned to two clusters: THY1+ C0 and THY1+ C1. **B** UMAP plot visualizing the expression of marker genes (THY1, TWIST1, PRRX1, and RXFP2) in THY1+ clusters of each tissue. Note that RXFP2 is expressed only in THY1+ C1 of AP-m and AP-f (Red arrowhead). **C** Male AP RNA velocity showing the differentiation trajectory of RXFP2+ cells to APPCs. The red arrowhead highlights the RXFP2+ cells in the original cell population.

regulated genes associated with G-protein-coupled receptor signaling, cell division, cell differentiation, calcium ion concentration, and neural crest cell development (Fig. 4M); the down-regulated genes were linked to epithelial-to-mesenchymal transition, positive regulation of cell death, and the response to hypoxia (Fig. 4N). These findings collectively support the crucial role of Wnt signaling in RXFP2+ APMCs activation for postnatal development of antlers.

Activation of male RXFP2+ APMCs requires participation of M2 macrophages recruited via released IL-34

Next, we utilized the CellChat tool to identify activated ligand-receptor pairs in RXFP2+ APMCs and other cell types. Comparing male AP to FP and LP respectively, we found that only one ligand-receptor pair, IL34-CSF1R, was significantly upregulated. These cells secrete the IL-34 cytokine, which targets macrophages expressing CSF1R, the macrophage colony-stimulating factor 1 receptor (Fig. 5A, B, Supplementary Fig. 5A). In this respect, IL-34 is known to induce differentiation of monocytes into macrophages[36] and can polarize macrophages to the M2 state[37]. IL-34 expression in male AP cells was further confirmed by immunofluorescence staining at the tissue level (Fig. 5C). Interestingly, we found that the MIF-CD74/CD44 and MIF-CD74/CXCR4 pairs were significantly down-regulated (Fig. 5A) in the RXFP2+ APMCs (as the source) and CSF1R+ macrophages (as the target). MIF is a macrophage migration inhibitory factor, suggesting that the down-regulation of MIF in RXFP2+ APMCs may further stimulate macrophage migration and activation. In contrast, when comparing female AP to FP and LP respectively, we failed to detect significant up-regulation of the IL34-CSF1R pair (Supplementary Fig. 5B).

In further work, we re-examined the scRNA-seq data and identified M1 and M2 macrophages in these periosteal tissues (Fig. 5D, Supplementary

Fig. 5C, D). The male AP had the highest proportion of M2 macrophages, followed by the female AP, with the FP and LP having the lowest proportion of M2 macrophages (Fig. 5E, Supplementary Fig. 5E). In contrast to M2 macrophages, there were no significant changes in CSF1R expression in M1 macrophages across these four tissue types (Fig. 5F). However, CSF1R expression was significantly elevated in M2 macrophages resident in both male and female AP.

To investigate the role of the IL34-CSF1R pair in the initiating antler in vivo, we transplanted AP tissue subcutaneously onto the forehead of nude mice, to create a xenogeneic antler. The treatment group received intravenous injections of the CSF1R inhibitor (CSF1R-IN-3), while the control group, which also developed xenogeneic antlers, did not receive the inhibitor. Twenty-one days after treatment, there were no M2 macrophages in the CSF1R-IN-3 group detected and no cartilage tissue was observed in the xenogeneic antlers (Fig. 5G); also, the weight of the antlers was significantly lower in the treated group compared to the control group (Fig. 5H); however, M2 macrophages were found in the control group (Supplementary Fig. 5F). Therefore, these results indicate that male RXFP2+ APMCs have the ability to recruit M2 macrophages via release of IL-34, and M2 macrophages are likely involved in the activation of RXFP2+ APMCs. In one of our previous studies, we created xenogeneic antlers in fluorescent nude mice, and found that all the immune cells within these xenogeneic antlers were labeled with red fluorescent dye, indicating that these cells were derived from the host mouse[38].

RXFP2+ APMCs exhibit significantly lower HOXD gene expression levels

HOX genes play a key role in determining the developmental pattern of organism. To investigate the expression patterns and levels of HOX genes
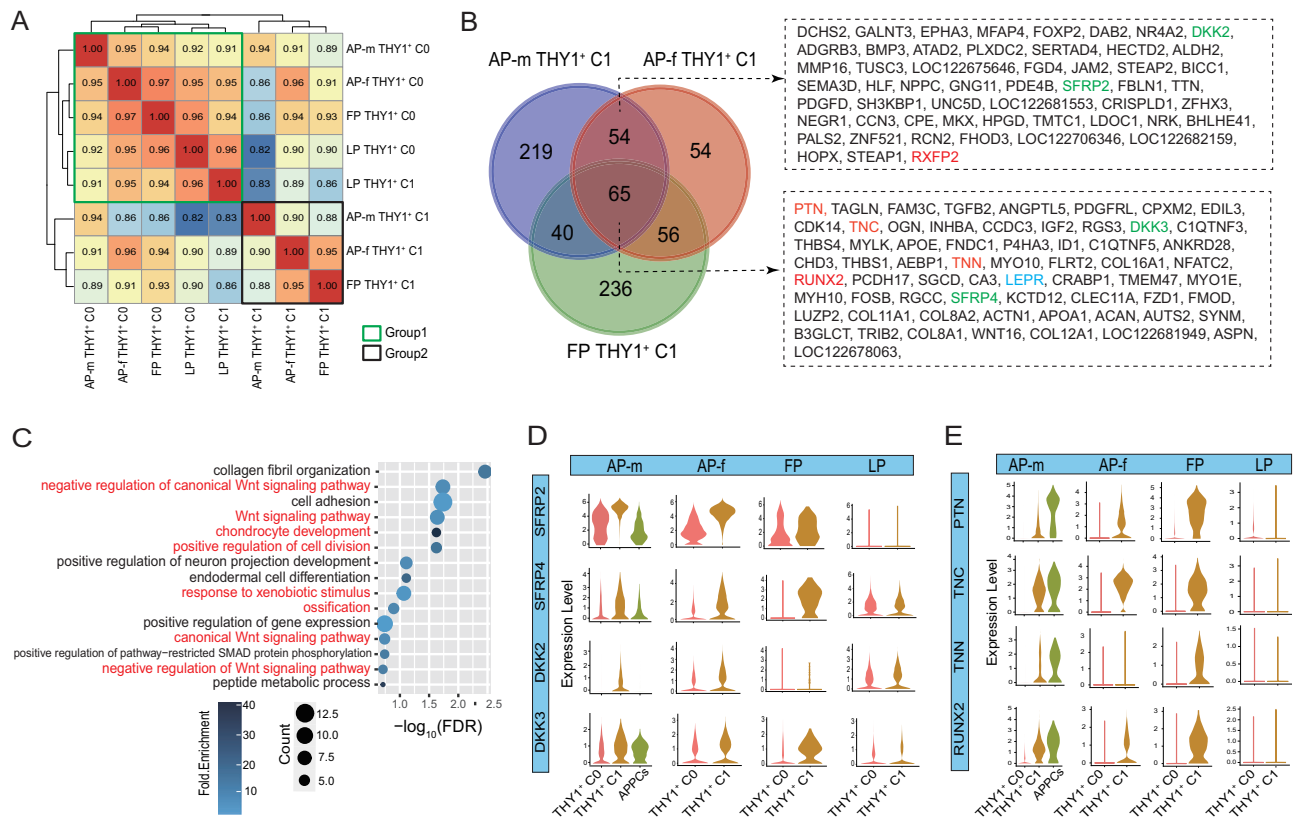
Fig. 3 | Inhibition of Wnt signaling is involved in male and female THY1+ C1. **A** Heat map showing correlations between THY1+ clusters of each tissue based on scRNA-seq data. Pearson correlation coefficients are displayed. **B** Venn diagram showing highly expressed genes of THY1+ C1 among AP-m, AP-f, and FP. The 54 genes of THY1+ C1 between AP-m and AP-f and the 65 genes of THY1 + C1 among AP-m, AP-f, and FP are shared and highlighted by a red dashed box. Genes that are highly relevant to the context of the study are highlighted in colors. **C** Dot plot showing DAVID-enriched Gene Ontology terms using 119 (54 + 65) shared highly expressed genes of THY1+ C1. **D** Violin plot showing the expression of WNT inhibitors (SFRP2, SFRP4, DKK2, and DKK3) in THY1+ clusters of each tissue and APPCs. Note the significantly high expression levels of these WNT inhibitors in THY1+ C1 among AP-m, AP-f, and FP. **E** Violin plot showing the expression of signature genes of APPCs (RUNX2, TNC, TNN, and PTN) in THY1+ clusters of each tissue and APPCs. Note that these signature genes are not expressed in LP.

in these periosteal tissues, we generated HOX gene expression profiles in male and female AP tissues and compared them with FP and LP tissues using bulk RNA-seq data. Our analysis revealed distinctive expression profiles: HOXA 5/6/7/8/9/10/11/13 were predominantly expressed in LP, while the HOXB and HOXC families were not expressed in any of the four periosteal tissues (Fig. 6A). HOXD 3/4/8/9 were expressed across all periosteal tissues, with HOXD 10/11/12/13 being primarily expressed in LP. The results of analysis of scRNA-seq data further support the above findings (Fig. 6B). Notably, within male and female APMCs and FPMCs, HOXD 1/3/4/8 tended to be expressed in RXFP2- APMCs compared to RXFP2+ APMCs (Fig. 6C). Next, we investigated the expression profiles of HOX genes in bone marrow mesenchymal cells (BMSCs) and RXFP2+ APMCs (Fig. 6D) by analyzing scRNA-seq data of LEPR+ BMSCs from previously published human[39] and mouse scRNA-seq data[40] (Supplementary Fig. 6A, B). Notably, after normalizing these data, LEPR+ BMSCs exhibited significantly higher expression levels of HOX genes, especially the HOXA and HOXC families (Fig. 6E).

Comparison RXFP2+ APMCs to LEPR+ BMSCs at the marker gene level

We further compared the expression status of key marker genes between RXFP2+ APMCs and LEPR+ BMSCs. These markers included those for generic mesenchymal cells, CNCC-derived mesenchymal cells, as well as osteogenic, chondrogenic, and adipogenic cells (Supplementary Fig. 6C). Interestingly, using the widely recognized mesenchymal cell markers, LEPR, THY1 (CD90), NT5E (CD73) and ENG (CD105), we found that these were expressed in both RXFP2+ APMCs and LEPR+ BMSCs. CNCC-derived

mesenchyme markers, such as TWIST1, PRRX2, and SNAI1, were highly expressed in RXFP2+ APMCs but were almost absent in BMSCs. With respect to lineage-specific markers, RXFP2+ APMCs mainly expressed transcription factors related to early differentiation, such as RUNX2 (osteogenic) and SOX9 (chondrogenic). However, adipogenic markers (e.g., CEBPA, FABP4, and LPL) were not expressed in RXFP2+ APMCs, but were highly expressed in BMSCs. These results indicate that although both RXFP2+ APMCs and LEPR+ BMSCs possess the capabilities for multi-lineage differentiation, their transcriptional heterogeneity is quite significant.

Discussion

Although the AP has been convincingly demonstrated to be the key tissue type that gives rise to postnatal development of antler through tissue dele-tion and transplantation experiments[7,20,22], Ba et al. (2022) found that the AP cells are heterologous and consist of eight cell populations; among these, the THY1+ mesenchymal cells was predicted to be the key. In another study[34], we identified a population of progenitor cells from the antler regeneration blastema and termed them antler blastema progenitor cells (ABPCs). These ABPCs are driven by PRRX1* mesenchymal cells. Both THY1 and PRRX1 are generic mesenchymal marker genes and are also expressed in the FPMCs and the LPMCs (Fig. 2B). Therefore, neither meets the criteria for a unique marker for the mesenchymal cells that resides exclusively in the AP. In the present study, we identified RXFP2 as a specific gene marker for labeling the distinctive antlerogenic cells, RXFP2+ APMCs. Importantly, this gene, RXFP2, was not expressed in the numerous deer tissues tested, including the FP, LP and 17 other types of deer tissue, and importantly, it was also not
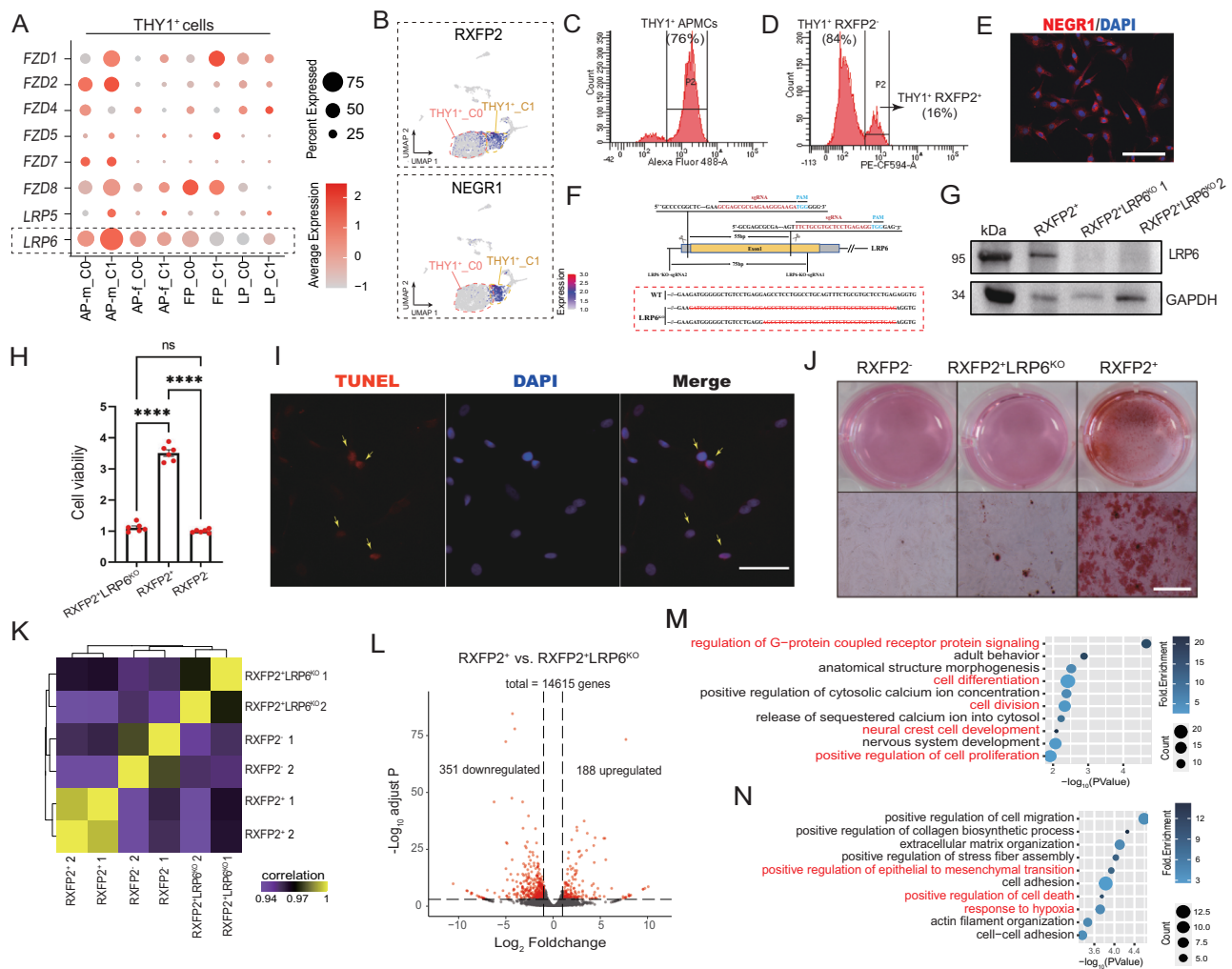
Fig. 4 | Effects of Wnt signaling knockdown in THY1⁺RXFP2⁺ APMCs. A Dot plot showing the expression of WNT receptors and co-receptors in THY1⁺ clusters of each tissue. **B** UMAP plot visualizing the expression of RXFP2 and NEGR1. Note that the expression patterns of these two genes are very similar. **C** Flow cytometry assay showing the proportion of THY1⁺ APMCs (76%) in the male AP tissue. **D** Flow cytometry assay showing the proportion of THY1⁺RXFP2⁺ APMCs (16%) and THY1⁺RXFP2⁻ APMCs (84%) in the THY1⁺ APMC population. **E** Immunofluorescence staining assay of NEGR1⁺ APMCs, indicating that the sorting of RXFP2⁺ cells was successful. Scale bar: 100 μm. Note that NEGR1 is exclusively expressed in male AP RXFP2⁺ APMCs. **F** Schematic showing the design of sgRNA to knock down part of exon 1 of LRP6 using CRISPR technology. **G** Immunoblots of LRP6 protein of RXFP2⁺LRP6^KO and RXFP2⁺ APMCs and internal reference protein (GAPDH) in the AP-m tissue. **H** Comparison of cell viability of three types of THY1⁺ APMCs. Note that the proliferation of RXFP2⁺ APMCs increased significantly compared to RXFP2⁻ APMCs and RXFP2⁺LRP6^KO APMCs. ****$p < 0.0001$. Error bars indicate the SEM. **I** Cell apoptosis rate of RXFP2⁺LRP6^KO APMCs through TUNEL assay analysis. Note that there is almost no cell apoptosis for RXFP2⁻ APMCs and THY1⁺RXFP2⁺ APMCs. Yellow arrowhead: apoptotic cells. **J** Osteogenic ability of three types of THY1⁺ APMCs through Alizarin red staining. Note that the osteogenic ability of RXFP2⁺ APMCs increased significantly compared to RXFP2⁻ APMCs and RXFP2⁺ LRP6^KO APMCs. **K** Heat map showing correlations between RXFP2⁺ APMCs, RXFP2⁻ APMCs and RXFP2⁺ LRP6^KO APMCs based on bulk RNA-seq data. Pearson correlation coefficients are displayed. **L** Volcano plot showing the DEGs in RXFP2⁺ APMCs vs. RXFP2⁺LRP6^KO APMCs. DEGs (dot) with an absolute log₂FoldChange > 2 and an adjusted p value < 0.001 are highlighted in red. Note that 188 genes are up-regulated and 351 are down-regulated. **M** Dot plot showing top DAVID-enriched Gene Ontology terms with 188 up-regulated genes in RXFP2⁺ APMCs vs. RXFP2⁺LRP6^KO APMCs. The terms highly relevant to the context of the study are highlighted in red. **N** Dot plot showing top DAVID-enriched Gene Ontology terms using 351 down-regulated genes in RXFP2⁺ APMCs vs. RXFP2⁺LRP6^KO APMCs. The terms highly relevant to the context of the study are highlighted in red.

expressed in the equivalent AP tissue in CWD, an antler-less deer species. Furthermore, through RNA velocity analysis, we found that the differentiation trajectory of RXFP2⁺ APMCs is clearly directed toward APPCs. Therefore, RXFP2⁺ APMCs can be considered as the reserved "seed" cells that are uniquely positioned in the AP tissue for the postnatal development of antlers.

As a secondary sexual characteristic, the initiation of the pedicle and the first antler formation takes place under the control of androgen hormones when male deer approach puberty[17,18]. Successful localization of the androgen hormone receptors (AR) in the AP tissue[41,42] demonstrates that androgen stimulation of pedicle formation may be through classical androgen/AR signaling pathway. Interestingly, androgen hormones, such as testosterone or dihydrotestosterone, failed to play a mitogenic role in stimulating proliferation of AP cells in vitro[33], indicating that some intermediate players may be involved in the process. In the present study, we detected high expression of Wnt signaling co-receptor LRP6 and found that knockdown of LRP6 via a CRISPR-cas9 approach significantly impaired proliferation rate of male RXFP2⁺ APMCs (RXFP2⁺LRP6^KO APMCs) compared to intact RXFP2⁺ APMCs, but was similar to that of RXFP2⁻ APMCs. It is reported that androgen/androgen receptor signaling can regulate Wnt/ß catenin either negatively in androgenetic alopecia[43] or positively in prostate cancer[44]. As another type of male secondary sexual
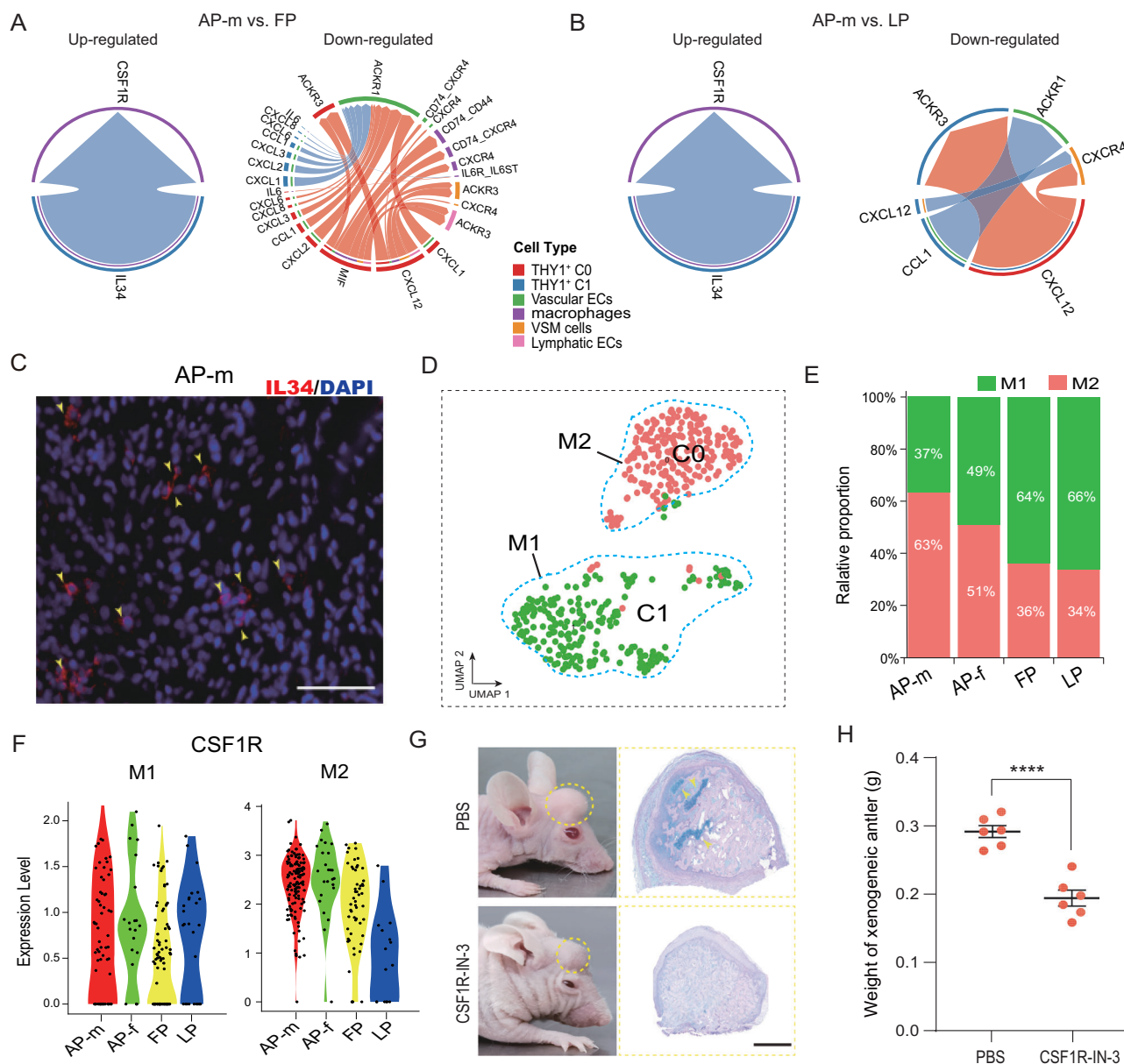
Fig. 5 | Male RXFP2+ APMCs recruit M2 macrophages via releasing IL-34.
A Circle plot showing up-regulated and down-regulated ligand-receptor pairs related to immune pathways comparing the male AP to the FP, respectively. Note that the IL34-CSF1R pair is significantly up-regulated in male AP, with RXFP2+ APMCs as the sender and the macrophages as the target. **B** Circle plot showing up-regulated and down-regulated ligand-receptor pairs related to immune pathways when comparing the male AP to the LP, respectively. **C** Immunofluorescence staining assay confirming the presence of IL-34 in male AP tissue. Yellow arrowhead: IL-34 secreting APMCs/APPCs. Scale bar: 100 μm. **D** UMAP plot visualizing two unsupervised clusters (C0 and C1) of macrophages in the four types of periosteum samples (AP-m, AP-f, FP, and LP). Note that C0 is annotated as M2 macrophages and C1 is annotated as M1 macrophages based on the known marker genes (Fig. S5C). **E** Bar plot showing the relative proportions of M1 and M2 macrophages

in the four types of periosteum samples. Note that the percentage of M2 macrophages is the highest in male AP among these periosteum tissues. **F** Violin plot showing expression levels of CSF1R (one of IL-34 receptors) in M1 and M2 macrophages of the four types of periosteum tissues. Note that CSF1R is significantly highly expressed in the M2 macrophages of male and female AP tissues. **G** Male AP tissue was transplanted into the forehead area of nude mice, and xenogeneic antlers formed gradually (left). Histological sections and H&E + Alcian blue staining of different xenogeneic antler groups showed that normal development (PBS group) resulted in the formation of large chondrocyte clusters, while in the CSF1R-IN-3 group (inhibitor of CSF1R), the majority of the formed xenogeneic antler was composed of fibrous connective tissue (right). **H** Weight of xenogeneic antlers is significantly different between the control and CSF1R-IN-3 groups. ****$p < 0.0001$. Error bars indicate the SEM.

characteristic, initiation of pedicle and first antler formation relies on androgen positive regulation of Wnt signaling.

We also showed that before activation of proliferation, RXFP2+ APMCs highly expressed Wnt signaling inhibitors (SFRP2, SFRP4, DKK2, and DKK3) and that these inhibitors were substantially down-regulated only when androgen hormone levels were significantly elevated during period of puberty to trigger initiation of pedicle formation. Wnt signaling is crucial for the expansion of skeletal progenitor cells and their differentiation

towards the osteoblast lineage[45]. Consistent with this finding, differentiation of RXFP2+ APMCs into APPCs occurred concurrently with a decrease in expression of Wnt inhibitors (Fig. 2F). Moreover, Wnt signaling knock-down in RXFP2+ APMCs resulted in a reduction in osteogenic potential (Fig. 5I). Previous studies have demonstrated the involvement of androgen-RXFP2 signaling in triggering THY1+ cells to differentiate into progenitor cells[29]. Therefore, the shift from Wnt signaling inhibition in RXFP2+ APMCs to its activation in APPCs may be associated with the regulation of
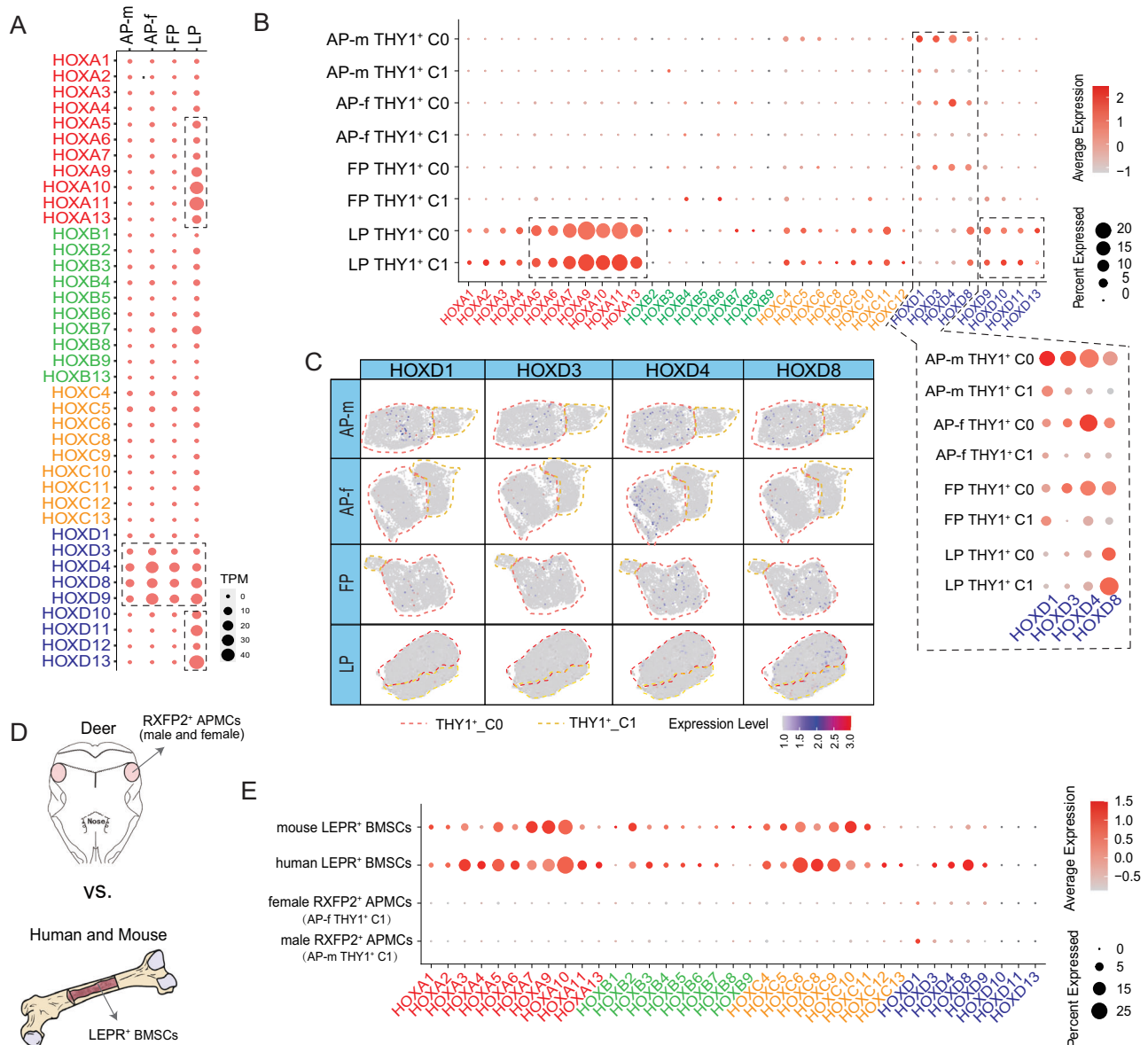
Fig. 6 | Expression profile of HOX genes. A Dot plot showing the expression of HOX genes in AP-m, AP-f, FP, and LP. Highly expressed HOX genes are highlighted by a black dashed box. **B** Dot plot showing the expression of HOX genes in THY1$^+$ clusters of these four types of tissues. Highly expressed HOX genes are highlighted by a black dashed box. Note that HOXD 1/3/4/8 are highly expressed in THY1$^+$ C0, but not in THY1$^+$ C1 for AP-m, AP-f, and FP. **C** UMAP plot visualizing the expression of HOXD 1/3/4/8 in THY1$^+$= clusters of AP-m, AP-f, and FP. **D** Schematic representation of deer RXFP2$^+$ APMCs and human and mouse LEPR$^+$ BMSCs. **E** Dot plot showing the expression of HOX genes in deer male and female RXFP2$^+$ APMCs and human and mouse LEPR$^+$ BMSCs. Note that HOX genes are highly expressed in LEPR$^+$ BMSCs.

androgen-RXFP2 signaling. In this respect, there is likely the potential for crosstalk between androgen-RXFP2 signaling and Wnt/ß catenin signaling in regulating differentiation of RXFP2$^+$ APMCs. Therefore, we propose that further studies should be directed at elucidating the mechanisms underlying such interactions between these two signaling pathways for the activation responsible for initiating the postnatal development of antlers.

Mesenchymal stem cells and macrophages are closely related partners[46–48]. On one hand, the mesenchymal stem cells regulate immune function by influencing proliferation, infiltration, and phenotypic polarization of immune cells, as well as osteoclast differentiation. On the other hand, immune cells, such as macrophages, stimulate the proliferation of mesenchymal stem cells and mediate their multipotent differentiation through modulation of their immune microenvironment. In our study, the IL34-CSF1R signaling pair was significantly upregulated in the male AP compared to FP and LP, with RXFP2$^+$ APMCs serving as the cytokine

source and macrophages as the target cells. IL-34 is a homo-dimeric secreted protein and a key ligand of the colony-stimulating factor receptor CSF-1R. It is well established that IL-34 regulates the proliferation, activation, survival, chemotaxis of mononuclear/macrophages[37] and promotes the differentiation of macrophages into the M2 phenotype[49,50]. Therefore, secretion of IL-34 in the case of the antler would be expected to recruit macrophages and polarize them to the M2 subtype, which in turn promote the differentiation of APMCs into cartilage, as we demonstrated using a nude mouse xenograft model in this study. Notably, Mao and colleagues have demonstrated that Wnt signaling up-regulates the level of IL34 in lupus nephritis patients[51]. This finding indicates that the crucial role of the immune microenvironment in postnatal antler development, specifically through interactions between RXFP2$^+$ APMCs and M2 macrophages.

It is known that HOX gene expression has negative impacts on cell differentiation plasticity (Leucht et al., 2008). The long bone periosteum is

mesoderm-derived and HOX-positive, while the cranial-facial periosteum is CNCC-derived and HOX-negative[52]. Studies have also convincingly shown that AP and its derivatives are CNCC-derived[53,54], and hence would be expected to show remarkably different plasticity compared to the LP. This aligns well with our findings in the present study in that one of the HOX family genes (HOXA) was highly expressed only in the LP. The expression pattern of RXFP2^{+} APMCs showed a negative correlation with expression of the HOXD gene.

Comparisons of RXFP2^{+} APMCs and BMSCs revealed that, while both expressed mesenchymal stem cell markers and share highly expressed genes indicative of multipotent differentiation potential, the RXFP2^{+} APMCs express additional signature genes associated with their CNCC origin. This may empower the RXFP2^{+} APMCs, a specialized cell population, with superior postnatal development potential compared to BMSCs, especially in the aspects of bone and cartilage development. Therefore, we propose that, for regenerative bone repair, CNCC-derived periosteal cells such as those from the cranial-facial periosteum, should be preferentially considered as a source of mesenchymal cells. These cells may offer a better opportunity for regenerative medicine compared to axial periosteum-derived cells, particularly for repair of the CNCC-derived bone defects[55].

In summary, this study contributes to our understanding of the postnatal development of secondary sexual characteristics, using deer antlers as an example. We successfully identified and isolated a pure subpopulation of cells with the exclusive potential to form antlers, revealing the mechanisms that regulate this cell population. Therefore, we believe that our work sheds light on the mechanisms underlying postnatal development related to secondary sexual characteristics as well as some other appendages or organs.

Methods

Ethical approval
The experimental protocols involving deer and mice were approved by the Ethics Committee of Changchun Sci-Tech University (Permit Number: CKARI202111). We have complied with all relevant ethical regulations for animal use.

Tissue sampling
Four types of periosteum tissues were collected from one-year-old sika deer immediately after slaughter. The dissection procedures followed methods outlined in a previous paper[56]. Briefly, for the female AP, each deer head was brought into the cell culture laboratory. The skin covering the frontal crest was surgically removed to expose the AP. An oval-shaped incision was made surrounding the crest using a scalpel, and the periosteum was peeled from the crest using rat-tooth forceps. The skin covering the long bone regions was opened to expose the LP, which was then peeled off using rat-toothed forceps. In total, six tissue samples were collected, with each tissue type having three biological replicates.

Bulk RNA-seq library construction, sequencing and analysis
Total RNA was isolated from the tissues and cells following standard protocols. One microgram (µg) of total RNA with a minimum RNA integrity number (RIN) of 7.0 was used to construct transcriptome sequencing libraries using the Illumina TruSeq RNA Library Preparation Kit v2 (Illumina, USA). After cleaning the raw data, and using the deer reference genome, we utilized the workflows of HISAT2, StringTie, and DESeq2[57] to analyze differentially expressed genes (DEGs) with $|\log_2 \text{FoldChange}| \geq 2$ and Benjamini-Hochberg p-value < 0.001 between two groups.

Cross-tissue/species comparison of RXFP2 expression levels
Data from our periosteum tissues and previously published sika deer transcriptome data[58,59] were incorporated into our analysis to perform a cross-tissue comparison. For cross-species comparison, our previously published data[60] were reanalyzed to investigate the expression levels of RXFP2 in AP tissues across antlered deer (sika deer, muntjac, reindeer) and antler-less Chinese water deer (CWD). Due to the lack of a high-quality genome for CWD, we performed de novo transcriptome assembly using the

workflows of Trinity v2.4.1[61], cd-hit-est v3.0.3[62], TransDecoder v2.0.1, and BLASTX to obtain RXFP2 mRNA sequences for each deer. However, assembling the RXFP2 mRNA sequence of the CWD in the AP-equivalent tissue was unsuccessful. Subsequently, FPKM (Fragments Per Kilobase of transcript per Million mapped reads) values for the RXFP2 mRNA sequences for each deer were estimated using RSEM v1.3.0[63].

Preparation of single-cell suspension
Fresh female AP and LP tissues were carefully dissected into small pieces measuring 1 mm³ using custom tools designed for this purpose[64]. Tissue segments were then transferred to a 50 ml centrifuge tube, where three individual samples of each tissue type were combined. The tissues were then incubated for preparation of single-cell suspensions as previously outlined[29].

Single-cell library construction and sequencing
Briefly, approximately 14,000 to ~20,000 single cells were diluted and mixed with a buffer following the manufacturer's guidelines. The cell mixture was loaded into 10X Chromium Controller, utilizing Chromium Single Cell 3' Reagent v3 reagents. Sequencing libraries were then prepared according to the manufacturer's instructions at Capitalbio Technology Corporation (Beijing, China). A 13-cycle cDNA amplification step was carried out to amplify the cDNA derived from the single cells. Subsequently, the resulting libraries were sequenced on an Illumina HiSeq 6000 platform.

Single-cell data processing
For each tissue, after aligning sequencing reads to the reference genome using Cell Ranger v6.1.2 from 10X Genomics, we conducted scRNA-seq data analysis using the R package Seurat v4.3.0[65]. To ensure high data quality, we implemented specific criteria: (1) inclusion of cells expressing more than 200 genes; (2) retention of genes expressed in at least 3 single cells; and (3) exclusion of cells with a mitochondrial gene percentage over 8% and cells with a ribosomal gene percentage over 30%. Additionally, potential doublets were removed using the R package DoubletFinder[66] to minimize noise and artifacts. To visualize the data, we first calculated the ratio of binned variance to mean expression for each gene and selected the top 3000 most variable genes. Next, we performed principal component analysis (PCA) and reduced the data to the top 30 PCs. We performed graph-based clustering of the previously identified PCs using the Louvain Method base on the same resolution parameter (0.1), and the clusters were visualized on a 2D map produced with UMAP. For each cluster, we used the Wilcoxon rank-sum test to identify significant DEGs when compared to the remaining clusters (Bonferroni correction was used to adjust for multiple hypothesis testing, adjusted p value < 0.01 was regarded as significant, paired tests when indicated). To visualize how well the cluster-specific DEGs (marker genes) defined each cluster, we constructed the feature plot (UMAP plot colored by expression level of indicated genes), and heatmap (top 50 genes with highest average log-transformed fold change - $\log_2$FC) using the Seurat R packages.

RNA velocity
scVelo[67] was employed to analyze RNA velocity by resolving the complete transcriptional dynamics of splicing kinetics. The scVelo approach employed a stochastic model aimed at more accurately capturing the steady states of gene expression.

Cell-cell signaling pathways
CellChat v2.1[68] was utilized to identify up-regulated and down-regulated signaling ligand-receptor pairs, with THY1^{+} cells as the sender and other cell types as targets, by performing an ultra-fast Wilcoxon test (threshold p < 0.05). The fold change for ligands and receptors was set at absolute $\log_2$FC > 0.1.

Gene set enrichment analysis
DAVID v2022q2[69] was used to identify significant terms for gene ontology. We considered terms with an adjusted Fisher exact p < 0.05.

Western blotting

Total proteins from tissues and cells were extracted using RIPA lysis buffer (Beyotime, Jiangsu, China). Proteins (20 μg per lane) were separated by 12% SDS-PAGE and transferred to PVDF membranes. Membranes were blocked with 5% skimmed milk powder and immunoblotted with primary antibodies RXFP2 (dilution: 1:500, custom-made by Abclonal, China) and LRP6 (dilution: 1:1000, A22661, Abclonal, China), followed by secondary antibodies (goat anti-rabbit IgG; dilution: 1:500, SE134, Solarbio, China) conjugated with horseradish peroxidase. Bands were visualized using enhanced chemiluminescence detection reagents (Thermo, USA) and a Chemiluminescent Imaging System (Tanon, China). Band quantification was performed using ImageJ software v2.1 and normalized to GAPDH.

Flow cytometry analysis, cell sorting and Immunofluorescence confirmation

Male AP cells were incubated with the primary antibody THY1 (dilution: 1:500, Cat. No: ab307736, Abcam, USA) for 2 h, followed by incubation with a secondary antibody (goat anti-rabbit IgG; dilution: 1:200, Cat. No: SA00013-2, Proteintech, China) for flow cytometry analysis using a BD FACSCelesta instrument. Fluorescence-minus-one (FMO) controls were used to establish gating strategies. Cell sorting was performed on a FACS Aria II system (BD Biosciences, USA), and data were analyzed with FlowJo software v10. To further refine the cell population, THY1$^+$ APMCs were incubated with the primary antibody RXFP2 (dilution: 1:200, custom-made by Abclonal, China) for 1.5 h, followed by a secondary antibody (goat anti-rabbit IgG; dilution: 1:200, Cat. No: SA00013-4, Proteintech, China), enabling the isolation of THY1$^+$RXFP2$^+$ APMCs and THY1$^+$RXFP2$^-$ APMCs. To confirm the effective isolation of RXFP2$^+$ cells, we incubated these cells with primary antibody NEGR1 (dilution: 1:250, Cat No: bs-11095R, Bioss, China), which co-expresses with RXFP2, followed by incubation with secondary antibodies (goat anti-rabbit IgG; dilution: 1:200, Cat No: SA00013-2, Proteintech, China) for 2 h. DAPI staining was performed for 5 min. Images were acquired and analyzed using an EVOS M5000 microscope (Thermo Fisher, USA).

Cell electroporation and screening

Approximately 20 μg of LRP6 specific sgRNA expression plasmid and 30 μg of NG-Cas9 plasmid were co-transfected into 3×10^6 RXFP2$^+$ APMCs using the NeonTM transfection system. The electroporation conditions for the RXFP2$^+$ APMCs were as follows: 13500 V, 30 ms, and 1 pulse. After 2 days, the cells were seeded into 100-mm dishes to form individual cell colonies. The cell clones were picked and cultured in 24-well plates. Approximately 15% of each cell clone was digested and lysed with 10 μl of NP40 lysis bufer (0.45% NP40 plus 0.6% proteinase K) for 1 h at 56 °C and 10 min at 95 °C to provide templates for genotyping. The primers for genotyping are shown as follows: LRP6 (forward 5′-TGGAAAGCTGG-GAAGCATGA-3′; reverse 5′-CATACAAAGCCCCTCGTCCC-3′).

Cell viability

Cell viability was assessed using the Cell Counting Kit-8 (CCK-8, Cat No: K1018, Apexbio, USA). Cells were initially cultured in DMEM medium for 2 days, followed by the addition of CCK-8 solution at a 10% volume ratio to DMEM medium for 1 h. The absorbance of the culture medium was measured at 450 nm using a microplate reader (Perlong, DNM-9606, China). Cell viability was evaluated by comparing absorbance values with those of the untreated control group.

Cell apoptosis

Cells were cultured in DMEM medium for 48 h and then subjected to the TUNEL assay (Cat No: C1089, Beyotime, China) according to the manufacturer's instructions to assess apoptosis.

Osteogenic differentiation

Cells were seeded into a 6-well cell culture plate at a density of 1×10^5 cells/ well with inducing reagent (Cat No: HUXMX-90021, OriCell, China). The formation and growth of bone nodules were analyzed at 21 days using Alizarin Red staining.

Xenogeneic antler mouse model assay

Nude mice (BALB/c-nu) were selected for xenogeneic antler model construction. The detailed procedure for AP tissue transplantation to nude mice was as our previous papers[22,70]. CSF1R-IN-3 (Cat No: HY-139990, MCE, USA) was injected into the tail vein at a dosage of 0.2 mg per day. CSF1R-IN-3 blocks CSF-1/CSF-1R signal transduction, suppressing macrophage migration and reprogramming M2 macrophages to the M1 phenotype. A 0.9% NaCl injection group served as the control. Each group consisted of six nude mice. After 21 days, the animals were euthanized using pentobarbital, and the xenogeneic antlers were halved. One half was fixed with 4% paraformaldehyde, embedded in paraffin, sectioned, and subjected to Hematoxylin-Alcian Blue staining to detect changes in chondrogenesis. The other half was prepared as frozen sections for immunofluorescence staining with primary antibodies CD11b (dilution: 1:200, Cat No: bsm-54156R, Bioss, China) and CD206 (dilution: 1:200, Cat No: A21014, Abclonal, China) to confirm the presence of M2 macrophages in the PBS group. Additionally, before AP tissue transplantation, AP tissue underwent immunofluorescence staining with the primary antibody IL34 (dilution: 1:100, Cat No: bs-18170R, Bioss, China).

Statistical analysis

Analysis of data was done using GraphPad software v5.0. Data are presented as mean ± standard error of mean (S.E.M.). Significant differences among three or more groups were determined using a one-way analysis of variance, followed by Tukey's multiple comparison tests.

Reporting summary

Further information on research design is available in the Nature Portfolio Reporting Summary linked to this article.

Data availability

The scRNA-seq gene expression profiling of female AP and LP from the this study have been deposited in OMIX, China National Center for Bioinformation/Beijing Institute of Genomics, Chinese Academy of Sciences (https://ngdc.cncb.ac.cn/omix) under accession numbers OMIX009035 and OMIX009036. The scRNA-seq data and bulk RNA-seq data of male AP and FP from the previous study have been deposited in the Sequence Read Archive (SRA) under accession number PRJNA750429. The bulk RNA-seq data of sika deer, muntjac, reindeer and CWD from the previous study have been deposited in SRA under accession number PRJNA768490. All source data corresponding to the relevant figures are provided in Supplementary Data 1.

References

1. Sun, Y. et al. Early puberty: A review on its role as a risk factor for metabolic and mental disorders. *Front. Pediatr.* **12**, 1326864 (2024).
2. Randall, V. A. Hormonal regulation of hair follicles exhibits a biological paradox. *Semin. Cell Dev. Biol.* **18**, 274–285 (2007).
3. Randall, V. A. Androgens and hair growth. *Dermatol. Ther.* **21**, 314–328 (2008).
4. Randall, V. A. et al. Do androgens influence hair growth by altering the paracrine factors secreted by dermal papilla cells?. *Eur. J. Dermatol.* **11**, 315–320 (2001).
5. Drife, J. O. Breast development in puberty. *Ann. NY Acad. Sci.* **464**, 58–65 (1986).
6. Li, C. & Suttie, J. M. Deer antlerogenic periosteum: A piece of postnatally retained embryonic tissue?. *Anat. Embryol.* **204**, 375–388 (2001).

7. Goss, R. J. & Powel, R. S. Induction of deer antlers by transplanted periosteum. I. Graft size and shape. *J. Exp. Zool.* **235**, 359–373 (1985).

8. Goss, R. J. *Deer Antlers. Regeneration, Function and Evolution*. (Academic Press, 1983).

9. Goss, R. J. Future directions in antler research. *Anat. Rec.* **241**, 291–302 (1995).

10. Kierdorf, U., Li, C. & Price, J. S. Improbable appendages: Deer antler renewal as a unique case of mammalian regeneration. *Semin. Cell Dev. Biol.* **20**, 535–542 (2009).

11. Li, C. in *19th Annual Queenstown Molecular Biology Meeting*. (ed Vic Arcus) 38.

12. Wang, D. & Landete-Castillejos, T. Stem cells drive antler regeneration. *Sci. (N. Y., NY)* **379**, 757–758 (2023).

13. Gomez, S. et al. Labeling studies on cortical bone formation in the antlers of red deer (Cervus elaphus). *Bone* **52**, 506–515 (2013).

14. Goss, R. J. Problems of antlerogesis. *Clin. Orthop. Relat. Res.* **69**, 227–238 (1970).

15. Gaspar-López, E. et al. Biometrics, testosterone, cortisol and antler growth cycle in Iberian Red Deer Stags (Cervus elaphus hispanicus). **45**, 243-249, https://doi.org/10.1111/j.1439-0531.2008.01271.x (2010).

16. Lincoln, G. A. Appearance of antler pedicles in early foetal life in red deer. *J. Embryol. Exp. Morphol.* **29**, 431–437 (1973).

17. Li, C., Littlejohn, R. P., Corson, I. D. & Suttie, J. M. Effects of testosterone on pedicle formation and its transformation to antler in castrated male, freemartin and normal female red deer (Cervus elaphus). *Gen. Comp. Endocrinol.* **131**, 21–31 (2003).

18. Suttie, J. M., Fennessy, P. F., Lapwood, K. R. & Corson, I. D. Role of steroids in antler growth of red deer stags. *J. Exp. Zool.* **271**, 120–130 (1995).

19. Li, C. & Suttie, J. M. Light microscopic studies of pedicle and early first antler development in red deer (Cervus elaphus). *Anat. Rec.* **239**, 198–215 (1994).

20. Hartwig, H. & Schrudde, J. Experimentelle Untersuchungen zur Bildung der primären Stirnauswüchse beim Reh (Capreolus capreolus L.). *Z. f.ür. Jagdwiss.* **20**, 1–13 (1974).

21. Kierdorf, U. & Kierdorf, H. Delayed ectopic antler growth and formation of a double-head antler in the metacarpal region of a fallow buck (Dama dama L.) following transplantation of antlerogenic periosteum. *Ann. Anat. = Anatomischer Anz. Organ Anatomische Ges.* **182**, 365–370 (2000).

22. Li, C., Harris, A. J. & Suttie, J. M. Tissue interactions and antlerogenesis: new findings revealed by a xenograft approach. *J. Exp. Zool.* **290**, 18–30 (2001).

23. Li, C. et al. Development of a nude mouse model for the study of antlerogenesis–mechanism of tissue interactions and ossification pathway. *J. Exp. Zool. B Mol. Dev. Evol.* **312**, 118–135 (2009).

24. Li, C. & Suttie, J. M. Electron microscopic studies of antlerogenic cells from five developmental stages during pedicle and early antler formation in red deer (Cervus elaphus). *Anat. Rec.* **252**, 587–599 (1998).

25. Berg, D. K., Li, C., Asher, G., Wells, D. N. & Oback, B. Red deer cloned from antler stem cells and their differentiated progeny. *Biol. Reprod.* **77**, 384–394 (2007).

26. Li, C. Deer antler regeneration: a stem cell-based epimorphic process. *Birth Defects Res C. Embryo Today* **96**, 51–62 (2012).

27. Li, C., Yang, F. & Sheppard, A. Adult stem cells and mammalian epimorphic regeneration-insights from studying annual renewal of deer antlers. *Curr. Stem cell Res. Ther.* **4**, 237–251 (2009).

28. Wang, D. et al. Deer antler stem cells are a novel type of cells that sustain full regeneration of a mammalian organ-deer antler. *Cell Death Dis.* **10**, 443 (2019).

29. Ba, H. et al. Single-cell transcriptome reveals core cell populations and androgen-RXFP2 axis involved in deer antler full regeneration. *Cell Regen. (Lond., Engl.)* **11**, 43 (2022).

30. Yuan, F. P. et al. The role of RXFP2 in mediating androgen-induced inguinoscrotal testis descent in LH receptor knockout mice. *Reprod. (Camb., Engl.)* **139**, 759–769 (2010).

31. Johnston, S. E. et al. Genome-wide association mapping identifies the genetic basis of discrete and quantitative variation in sexual weaponry in a wild sheep population. *Mol. Ecol.* **20**, 2555–2566 (2011).

32. Calamari, Z. T. & Flynn, J. J. Gene expression supports a single origin of horns and antlers in hoofed mammals. *Commun. Biol.* **7**, 509 (2024).

33. Li, C., Littlejohn, R. P. & Suttie, J. M. Effects of insulin-like growth factor 1 and testosterone on the proliferation of antlerogenic cells in vitro. *J. Exp. Zool.* **284**, 82–90 (1999).

34. Qin, T. et al. A population of stem cells with strong regenerative potential discovered in deer antlers. *Sci. (NY, NY)* **379**, 840–847 (2023).

35. Soldatov, R. et al. Spatiotemporal structure of cell fate decisions in murine neural crest. *Sci. (NY, NY)* **364**, eaas9536 (2019).

36. Boulakirba, S. et al. IL-34 and CSF-1 display an equivalent macrophage differentiation ability but a different polarization potential. *Sci. Rep.* **8**, 256 (2018).

37. Foucher, E. D. et al. IL-34 induces the differentiation of human monocytes into immunosuppressive macrophages. antagonistic effects of GM-CSF and IFNγ. *PLoS One* **8**, e56045 (2013).

38. Wang, D. et al. Chimeric blood vessels sustained development of the xenogeneic antler: A unique model for xenogeneic organ generation. *Life Med.* **2**, https://doi.org/10.1093/lifemedi/lnac021 (2022).

39. Wang, Z. et al. Single-cell RNA sequencing deconvolutes the in vivo heterogeneity of human bone marrow-derived mesenchymal stem cells. *Int. J. Biol. Sci.* **17**, 4192–4206 (2021).

40. Baryawno, N. et al. A cellular taxonomy of the bone marrow stroma in homeostasis and leukemia. *Cell* **177**, 1915–1932.e1916 (2019).

41. Li, C., Bing, G., Zhang, X. & Zhou, J. Measurement of testosterone specific-binding (receptor) content of antlerogenic site periosteum in male and female sika deer. *Acta Veterinaria et. Zootechnica Sin.* **21**, 11–14 (1990).

42. Li, C., Harris, A. J. & Suttie, J. M. in *Recent Development in Biology of Deer* (ed J. A. Milne) (1998).

43. Premanand, A. & Reena Rajkumari, B. Androgen modulation of Wnt/β-catenin signaling in androgenetic alopecia. *Arch. Dermatol. Res.* **310**, 391–399 (2018).

44. Khurana, N. & Sikka, S. C. Interplay Between SOX9, Wnt/β-catenin and androgen receptor signaling in castration-resistant prostate cancer. *Int. J. Mol. Sci.* **20**, https://doi.org/10.3390/ijms20092066 (2019).

45. Mishina, Y. & Snider, T. N. Neural crest cell signaling pathways critical to cranial bone development and pathology. *Exp. Cell Res.* **325**, 138–147 (2014).

46. Arabpour, M., Saghazadeh, A. & Rezaei, N. Anti-inflammatory and M2 macrophage polarization-promoting effect of mesenchymal stem cell-derived exosomes. *Int. Immunopharmacol.* **97**, 107823 (2021).

47. Ren, G. et al. Mesenchymal stem cell-mediated immunosuppression occurs via concerted action of chemokines and nitric oxide. *cell Stem Cell* **2**, 141–150 (2008).

48. Zhang, F. F. et al. Interplay between mesenchymal stem cells and macrophages: Promoting bone tissue repair. *World J. Stem Cells* **16**, 375–388 (2024).

49. Muñoz-Garcia, J. et al. The twin cytokines interleukin-34 and CSF-1: Masterful conductors of macrophage homeostasis. *Theranostics* **11**, 1568–1593 (2021).

50. Jeannin, P., Paolini, L., Adam, C. & Delneste, Y. The roles of CSFs on the functional polarization of tumor-associated macrophages. *FEBS J.* **285**, 680–699 (2018).

51. Mao, Y. J., Qin, S. & Jiao, Z. F. Wnt pathway regulates IL-34 level in lupus nephritis. *Eur. Rev. Med. Pharmacol. Sci.* **23**, 5360–5365 (2019).

52. Leucht, P. et al. Embryonic origin and Hox status determine progenitor cell fate during adult bone regeneration. *Development* **135**, 2845–2854 (2008).

53. Landete-Castillejos, T. et al. Antlers - Evolution, development, structure, composition, and biomechanics of an outstanding type of bone. *Bone* **128**, 115046 (2019).

54. Ba, H. et al. Insights into the molecular characteristics of embryonic cranial neural crest cells and their derived mesenchymal cell pools. *Commun. Biol.* **7**, 1347 (2024).

55. Naung, N. Y., Duncan, W., Silva, R. D. & Coates, D. Localization and characterization of human palatal periosteum stem cells in serum-free, xeno-free medium for clinical use. *Eur. J. Oral. Sci.* **127**, 99–111 (2019).

56. Li, C., Clark, D. E., Lord, E. A., Stanton, J. A. & Suttie, J. M. Sampling technique to discriminate the different tissue layers of growing antler tips for gene discovery. *Anat. Rec.* **268**, 125–130 (2002).

57. Pertea, M., Kim, D., Pertea, G. M., Leek, J. T. & Salzberg, S. L. Transcript-level expression analysis of RNA-seq experiments with HISAT, StringTie and Ballgown. *Nat. Protoc.* **11**, 1650–1667 (2016).

58. Ba, H., Wang, D., Yau, T. O., Shang, Y. & Li, C. Transcriptomic analysis of different tissue layers in antler growth Center in Sika Deer (Cervus nippon). *BMC Genomics* **20**, 173 (2019).

59. Jia, B. Y. et al. Transcriptome analysis of sika deer in China. *Mol. Genet Genomics* **291**, 1941–1953 (2016).

60. Ba, H., Chen, M. & Li, C. Cross-species analysis reveals co-expressed genes regulating antler development in cervidae. *Front. Genet.* **13**, 878078 (2022).

61. Haas, B. J. et al. De novo transcript sequence reconstruction from RNA-seq using the Trinity platform for reference generation and analysis. *Nat. Protoc.* **8**, 1494–1512 (2013).

62. Li, W. & Godzik, A. Cd-hit: a fast program for clustering and comparing large sets of protein or nucleotide sequences. *Bioinformatics* **22**, 1658–1659 (2006).

63. Li, B. & Dewey, C. N. RSEM: accurate transcript quantification from RNA-Seq data with or without a reference genome. *BMC Bioinforma.* **12**, 323 (2011).

64. Chu, W., Zhao, H., Li, J. & Li, C. Custom-built tools for the study of deer antler biology. *Front Biosci. (Landmark Ed.)* **22**, 1622–1633 (2017).

65. Hao, Y. et al. Integrated analysis of multimodal single-cell data. *Cell* **184**, 3573–3587.e3529 (2021).

66. McGinnis, C. S., Murrow, L. M. & Gartner, Z. J. DoubletFinder: Doublet detection in single-cell RNA sequencing data using artificial nearest neighbors. *Cell Syst.* **8**, 329–337.e324 (2019).

67. Bergen, V., Lange, M., Peidli, S., Wolf, F. A. & Theis, F. J. Generalizing RNA velocity to transient cell states through dynamical modeling. *Nat. Biotechnol.* **38**, 1408–1414 (2020).

68. Jin, S. et al. Inference and analysis of cell-cell communication using CellChat. *Nat. Commun.* **12**, 1088 (2021).

69. Sherman, B. T. et al. DAVID: A web server for functional enrichment analysis and functional annotation of gene lists (2021 update). *Nucleic Acids Res.* **50**, W216–W221 (2022).

70. Li, C. et al. Role of heterotypic tissue interactions in deer pedicle and first antler formation-revealed via a membrane insertion approach. *J. Exp. Zool. B Mol. Dev. Evol.* **310**, 267–277 (2008).

Author contributions
C.L. and H.B. conceived and designed the research. Y.S., C.M. and Q.G. collected samples. P.H., H.Y., Z.W., D.W. and Q.G. performed experiments. H.B. analyzed and interpreted the data. C.L. and H.B. wrote and revised the manuscript. All authors have read and approved the final manuscript.

Competing interests
The authors declare no competing interests.

Additional information
Supplementary information The online version contains supplementary material available at https://doi.org/10.1038/s42003-025-08085-w.

Correspondence and requests for materials should be addressed to Hengxing Ba or Chunyi Li.

Peer review information *Communications Biology* thanks Tomas Landete-Castillejos, Maneeshi Prasad, and the other, anonymous, reviewer for their contribution to the peer review of this work. Primary Handling Editor: Dario Ummarino.

Reprints and permissions information is available at http://www.nature.com/reprints

Publisher's note Springer Nature remains neutral with regard to jurisdictional claims in published maps and institutional affiliations.